

Si(001) step dynamics: A temporal low-energy electron diffraction studyM. Kammler,¹ M. Horn von Högen,¹ N. Voss,² M. Tringides,² A. Menzel,³ and E. H. Conrad³¹*Fachbereich Physik, Universität Essen, 45117 Essen, Germany*²*Ames Laboratory, Iowa State University, Ames, Iowa 50011*³*School of Physics, Georgia Institute of Technology, Atlanta, Georgia 30332*

(Received 27 August 2001; published 30 January 2002)

We present equilibrium measurements of the dynamics of steps on Si(001) using temporal electron-diffraction spectroscopy. Activation energies and the rate limiting kinetics are identified for $950\text{ K} \leq T \leq 1130\text{ K}$. Unlike previous studies at higher temperatures, we can exclude evaporation and condensation of atoms or dimers from the step edges as the rate limiting process in this temperature regime. The possible reason for this difference is discussed in terms of a crossover from different rate-limiting kinetics.

DOI: 10.1103/PhysRevB.65.075312

PACS number(s): 68.03.Fg, 68.35.Fx, 61.14.Dc, 61.14.Hg

I. INTRODUCTION

Understanding crystal growth, how surface structures form or phase separate and how chemical reactions proceed, requires detailed information on surface kinetics. Scanning tunneling microscopy (STM) and field emission microscopy (FEM) have been able to extract activation energies, but STM and FEM are either done far from equilibrium, over limited temperature ranges (thus restricted time regimes), in the presence of finite electric fields, or over reduced length scales.^{1,2} Near-equilibrium kinetics measurements on macroscopic crystals that overcome these problems are sparse. Recently, however, the ability to measure near-equilibrium dynamic properties was demonstrated using temporal low-energy electron-diffraction spectroscopy (TLS).³

In this paper we present TLS measurements of the step dynamics of vicinal Si(001). Because the production of flat films requires a clear understanding of atomic step flow, step dynamics is an active research field. Step kinetics on Si(001) has been studied using a number of techniques.^{4–8} The eventual goal of all these experiments is to identify the key microscopic processes responsible for step motion within different temperature ranges. Previous works investigated equilibrium step kinetics either above 1000 K or below 600 K, with a few nonequilibrium measurements carried out near 800 K. There is some consensus between these studies that detachment of atoms or dimers from the step edges is the rate-limiting process. In this work we have studied the equilibrium step kinetics of Si(001) in the temperature range $950\text{ K} \leq T \leq 1130\text{ K}$. As in previous work, we show that continuum models for step fluctuations are adequate to describe the step fluctuations. However, contrary to work at higher and lower temperatures, we find that diffusion of atoms or dimers along the step edges is the rate-limiting process in this temperature range. In this paper, we present the results of our TLS study on step kinetics. We also compare our results with those from low-energy electron microscopy (LEEM) carried out at higher temperatures ($T \geq 1050\text{ K}$) where the rate-limiting process was determined to be the evaporation of atoms or dimers from step edges to terraces.⁸ As we will show, interpretations of previous LEEM results are in fact consistent with the findings reported in this paper. Furthermore, they suggest that the dynamics of steps and

islands on Si(001) are quite complicated, involving crossovers from one type of kinetics to another in different temperature regimes.

A TLS experiment measures the diffraction intensity, $I(\vec{q}, t)$, as a function of time for a particular momentum transfer vector \vec{q} . Fluctuations in $I(\vec{q}, t)$ are due to surface structural fluctuations determined by the choice of \vec{q} . For stepped surfaces with an average step spacing L , \vec{q} is chosen to correspond to an out-of-phase condition, so that adjacent terraces scatter destructively, making $I(\vec{q}, t)$ sensitive to the step-edge position.⁹ Thus the time sequence of the diffraction intensity contains information on the dynamics of the steps.

For pulse counting, a discrete-time series $I[n]$ is generated from $I(\vec{q}, t)$ by summing pulses from the electron multiplier over both the gate period t_g , and the diffractometer resolution $\Delta\vec{q}$. Here $t = nt_g$. From the series $I[n]$, the autocovariance function $\hat{G}[m]$ is generated:

$$\hat{G}[m] = \langle \delta I[n] \delta I[n+m] \rangle, \quad (1)$$

where $\delta I[n] = I[n] - \langle I \rangle$, and $\langle I \rangle$ is the average number of counts per gate time. The brackets, $\langle \dots \rangle$, represent a time average over the collection time $t_c = Nt_g$ (N is the number of data points in the time series). Although $\hat{G}[m]$ is not strictly equivalent to the true autocovariance function $G(\tau)$ ($\tau = mt_g$) for an infinite time series, we will use the two definitions interchangeably.¹⁰ The differences between $\hat{G}[m]$ and $G(\tau)$ can be estimated with reasonable accuracy as long as t_c is sufficiently long compared to the characteristic decay of $G(\tau)$.

It can be shown that $G(\tau)$ contains all of the kinetic information in a TLS experiment.¹¹ For instance, the characteristic decay time of $G(\tau)$, $\tau_{1/2}$, gives information about the diffusion barriers, while the functional form of $G(\tau)$ gives information about the microscopic mechanism driving the surface dynamics.

A number of continuum models describing the dynamics of steps exists.^{12,13} Common to all these models is a stochastic microscopic driving force that causes local fluctuations in the step position and a restoring force that tends to keep the steps straight. The driving force is parametrized by a step mobility Γ that depends on the type of kinetics. There are

two terms to the restoring force. As the step fluctuates, kinks form on the step edges. Since this costs energy, there is a force to straighten the step and thus lower the total kink energy. This part of the restoring force is parametrized by the step-edge stiffness $\tilde{\beta}(T)$,^{12–15}

$$\tilde{\beta}(T) = \frac{a_{\parallel} kT}{b^2(T, \epsilon)}, \quad (2)$$

where $b^2(T, \epsilon)$ is the step diffusivity that depends on the kink formation energy ϵ and on the model for kink formation.^{12,14,16} a_{\parallel} is the minimum length of a kink parallel to the step edge, and a_{\perp} is the kink length perpendicular to the steps.

In addition to the step-edge stiffness, there is also a local constraining potential per step length, $U(x)$, due to interactions between neighboring steps separated by x . Fluctuations in the step position must do work against this potential, and thus this term tends to keep the steps straight. For small fluctuation amplitudes Δx , the interaction energy $V(\Delta x, L)$ for steps with a mean separation L can be approximated by¹⁵

$$V(\Delta x, L) \approx 2U(L) + c(L)\Delta x^2, \quad (3a)$$

where

$$c(L) = \partial^2 U / \partial x^2|_L. \quad (3b)$$

The constant $c(L)$ is used as the second parameter in determining the restoring force.

Both $\tilde{\beta}$ and c govern two equilibrium properties of the step: the mean-squared step displacement w_{∞}^2 , and the correlation length along the step, ξ . In a continuum model,^{11,12,15}

$$w_{\infty}^2(T) = kT \left(\frac{1}{8c\tilde{\beta}} \right)^{1/2}, \quad (4a)$$

$$\xi(T) = \left(\frac{\tilde{\beta}}{2c} \right)^{1/2}. \quad (4b)$$

For stepped Si(001) the three kinetics models for step motion that determine the step mobility are step-edge diffusion (SD), terrace diffusion (TD), and evaporation/condensation (EC). The evaporation and condensation of atoms or dimers to and from the step edges provides a source or sink of diffusing species. Once detached from the steps, they can either diffuse along the steps or across the terraces to reattach to the steps, causing a fluctuation in the step shape. The EC process will therefore be the rate-limiting process when either diffusion along the steps or across the terraces are fast compared to the evaporation/condensation rate. In this case the step mobility is given by $\Gamma = \Omega^{3/2} / \tau_a$, where Ω is the dimer area ($\Omega = a_{\parallel} a_{\perp} = 0.289 \text{ nm}^2$), and τ_a is roughly the time for detachment/attachment of a dimer to the step.¹²

On the other hand, if the EC process is fast compared to both terrace and step-edge diffusion, either the TD or SD processes will determine the rate-limiting kinetics. In the limit of fast EC kinetics, terrace diffusion will determine the

time scale for step fluctuation if step-edge diffusion is much slower than terrace diffusion. The step kinetics are determined by the terrace diffusion constant D_t and the equilibrium concentration of the diffusion species on the terraces, c_o . The step mobility for terrace diffusion is then $\Gamma_t = 2D_t c_o \Omega^{3/2}$.¹³

Finally, for fast EC kinetics the SD process will determine the step fluctuations if step-edge diffusion is faster than terrace diffusion. The step kinetics are then governed by the diffusion constant D_s along the step edges ($D_s = \Omega / \tau_s$, where τ_s is the time to hop between adjacent sites on the step edge). The step mobility for SD kinetics is $\Gamma_s = \Omega^{1/2} D_s$.¹²

Using these models for the statistics of the step-edge positions, the statistics of $I(\vec{q}, t)$ can be calculated from which $G(\tau)$ is determined.¹¹ Based on numerical calculations the long-time behavior of $G(\tau)$ is determined by the rate-limiting kinetics, and can be summarized by a single equation. For τ greater than the characteristic decay time of $G(\tau)$, $\tau_{1/2}$, the correlation function decays as^{11,17}

$$G(\tau) \propto \exp[-A(n)(\tau/\tau_o)^{1/n}], \quad (5)$$

where $A(n)$ and τ_o are constants that depend on n , and will be discussed later in Sec. III B.¹¹ The microscopic kinetics determine n in Eq. (5): $n=1$ for EC kinetics, $n=3$ for TD kinetics, and $n=4$ for SD kinetics. Therefore, measuring the functional decay of $G(\tau)$ allows the microscopic mechanism for step motion to be determined. As we will show, TLS is capable of distinguishing these functional forms.

II. EXPERIMENT

Data were taken using a spot profile analysis low-energy electron-diffraction (SPA LEED) system with an external electron gun operating at 300 eV.¹⁸ The system transfer widths were $\zeta \sim 400$ and 1600 \AA , parallel and perpendicular to the steps, respectively. The Si(001) sample was cut with its surface normal tilted $\sim 1^\circ$ toward the [110] direction, producing $\langle L \rangle = 65 \text{ \AA}$ terraces. The sample was cleaned using standard techniques.¹⁹ Time series data were taken at an out-of-phase condition: $q_z = 6.93 \text{ \AA}^{-1}$ and $q_x = 0.0455 \text{ \AA}^{-1}$ [q_z and q_x denote momentum transfers normal to the (110) terraces and perpendicular to the step edges, respectively]. For all data the gate period was $t_g = 2 \text{ ms}$. A single time series consisted of $N = 9000$ points (a collection time, $t_c = 18 \text{ s}$). At each temperature $\hat{G}[m]$ was generated and ensemble averaged over 200 individual correlation functions. Each function $\hat{G}[m]$ in the ensemble was weighted by $1/\langle I \rangle^2$.¹¹

The bulk symmetry and the 2×1 phase of Si(001) cause adjacent terraces to alternate between dimers parallel and perpendicular to the steps. This leads to two types of steps: a relatively smooth S_A step and a rough S_B step (see Fig. 1). Dimers on the upper terraces are parallel and perpendicular to the S_A and S_B steps, respectively.^{4,13}

III. RESULTS

A. Static energies

Before discussing the step kinetics, it is important to mention how static energies and the correlation length along a

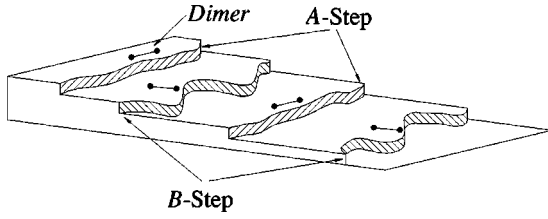


FIG. 1. Schematic of the stepped Si(001) surface showing both the S_A and S_B steps and the relative dimer orientation.

step are obtained. These static measurements confirm that the continuum models used in the analysis of the kinetics data produce reasonable results. As the amplitude of the step fluctuations increases with temperature, the decreased correlation along the steps causes the diffraction peaks to broaden in the direction parallel to the step edges. The broadening of these peaks is directly proportional to ξ^{-1} .¹⁴ Therefore, from Eq. (4b) the peak widths give information on the ratio $\tilde{\beta}/c$.

Figure 2 shows diffraction profiles perpendicular and parallel to the step edges at an out-of-phase condition (q is given in units of percent of the Brillouin zone $2\pi/a$: $a = 3.84 \text{ \AA}$). In the inset of Fig. 2 the peak splitting perpendicular to the steps is shown where the peak separation is $\Delta q_x = 2\pi/L$. Figure 2 is a profile parallel to the steps taken through the peak marked by the dashed line in the inset of Fig. 2, i.e., $q_x = 2.78\% \text{ BZ}$.

For Si(001), S_A and S_B steps fluctuate but with different amplitudes.^{4,20} Assuming that adjacent steps are independent, the diffraction line shapes will consist of two components: a sharp term whose width is related to the straighter S_A steps, and a broad component related to the coarser S_B steps. The solid line in Fig. 2 is a two-component fit: a broad Lorentzian due to larger fluctuating S_B steps, and a narrow Gaussian for straighter S_A steps. The dashed line in Fig. 2 is a single

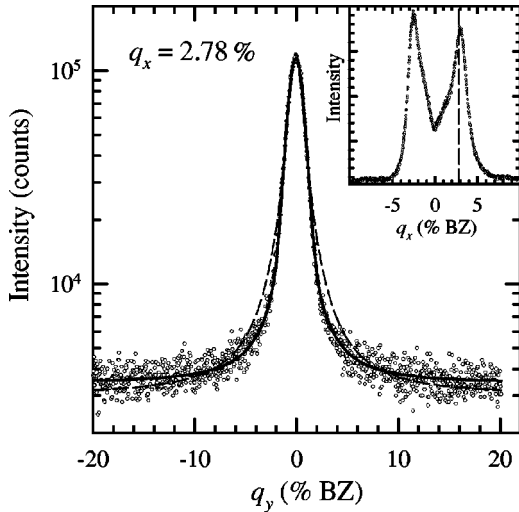


FIG. 2. Intensity profile parallel to the steps. (○) data. The solid line is a two-component fit, as described in the text. The dashed line is a single Lorentzian fit. The inset shows the intensity profile perpendicular to the steps for $T = 1023 \text{ K}$ showing peak splitting. The dashed line in the inset marks the value of q_x where the profile was taken.

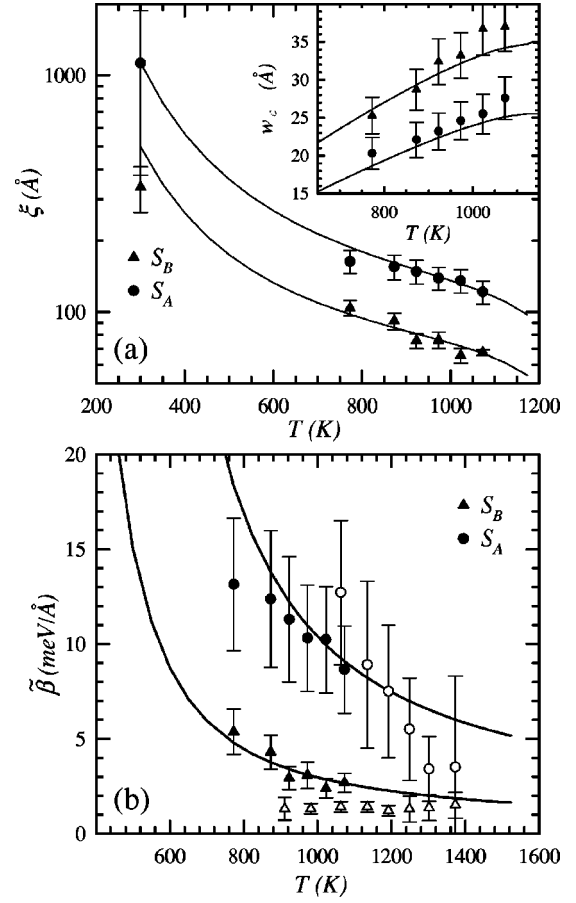


FIG. 3. The correlation length (a) and step stiffness (b) vs temperature. Solid symbols are those measured from this work, and open symbols are those measured in Ref. 21. Solid lines are best fit-values based on a TSK+corner model for b^2 and step-step interaction c . The inset in (a) shows the mean step fluctuation.

Lorentzian fit showing the poor quality of a fit without two components. The widths of each component were measured as a function of temperature to give ξ for both the S_A and S_B steps.¹⁴ Figure 3(a) shows the measured ξ as a function of temperature.

From the temperature dependence of ξ , we can estimate the step stiffness and the step-step interaction energy. To do this we must assume a model for b^2 in Eq. (2). A reasonable choice is the terrace-step-kink (TSK) model with corner energy that gives.¹⁴

$$b^2 = 2a_{\perp}^2 \frac{\sinh^{-2}(\epsilon/2kT)}{1 + \tanh(\epsilon/2kT)[\exp(\epsilon_c/2kT) - 1]}, \quad (6)$$

where ϵ and ϵ_c are the kink and corner energies, respectively. Since there are two types of steps, we assume that ϵ is different for each type of step. At the same time we will assume that ϵ_c and c are the same for both types of steps. Using ϵ_A , ϵ_B , ϵ_c , and c as fitting parameters, we can calculate $\xi(T)$ from Eqs. (2) and (4b), and compare the calculated value of ξ to the experimental values using a χ^2 routine. These fits are shown as solid lines for both the S_A and S_B steps in Fig. 3(a). The step-step interaction term is found to be $cL^2 = 1.2$

$\pm 0.2 \text{ meV}/\text{\AA}$. For the S_A step we find $\epsilon_A = 65 \pm 6 \text{ meV}$, while for the S_B step $\epsilon_B = 38 \pm 5 \text{ meV}$. The corner energy found is $\epsilon_c = 80 \pm 20 \text{ meV}$. The error in ϵ_c is large, although our fitted value is fortuitously equal to previous measurements.⁴

The values for the kink energies are in good agreement with earlier work using both STM and LEEM.^{4,8} Swartzentruber *et al.*⁴ found $\epsilon_A = 90 \pm 10 \text{ meV}$, while for the S_B step $\epsilon_B = 28 \pm 2 \text{ meV}$. While our S_A step kink energy is significantly lower than that of Swartzentruber *et al.*, Bartelt and Tromp⁸ found $\epsilon_A = 70 \pm 10 \text{ meV}$, within error bars of our result. From the measured ξ 's and our fit value for c , we can calculate $\tilde{\beta}$. The results are shown in Fig. 3(b). For comparison we have also plotted $\tilde{\beta}$ from a slightly higher temperature regime determined by LEEM.²¹ Our S_A step results are in good agreement with the LEEM results, while our S_B step stiffness is about 50% higher at 800 K. However, our extrapolated $\tilde{\beta}$ approaches the LEEM values above 1200 K.

We also note that the step-step interaction is also within error of those derived from strained Si(001) experiments.²² For a logarithmic step interaction potential $U(x) = C_1 + C_2 \ln(x/a)$,^{22,23} the elastic constant C_2 is given by $C_2 = cL^2$ [see the definition of c in Eq. (3b)]. From strained Si(001) experiments a value $C_2 = 1.17 \pm 0.17 \text{ meV}/\text{\AA}$ is found, in excellent agreement with our results.

There are two important observations that should be made about the amplitude of the step fluctuations, w_∞^2 . The inset in Fig. 3(a) shows w_∞ derived from $\tilde{\beta}$ and c . Using STM, Swartzentruber *et al.*²⁰ measured the terrace distribution of stepped Si(001) quenched from 875 K. From their measured terrace width distribution for surfaces with a mean terrace size of 67 \AA a value of $w_\infty \sim 26 \text{ \AA}$ can be extracted. This is in excellent agreement with our measurements, as seen in the inset in Fig. 3(a). Swartzentruber *et al.*²⁰ found that, for mean terrace sizes greater than 67 \AA , step collisions are rare and the terrace distribution is very well described by a step fluctuating between two fixed steps. This observation validates the assumption leading to Eq. (5), i.e., that even for 69 \AA terraces the steps can be thought of as fluctuating independent of their neighbors.¹¹

The other observation is that w_∞ is approximately 1.5 times larger for S_B steps than for S_A steps over the entire range of the experiment. Since the magnitude of the TLS signal is quadratic in w_∞^2 [i.e., $G(\tau) \propto w_\infty^4$ (Ref. 11)], the majority of the TLS signal comes from the S_B step fluctuations. In subsequent discussions of the Si(001) step kinetics, we will refer to activation energies and prefactors as being those of S_B steps.

B. Kinetics of stepped Si(001)

Figure 4 shows the normalized autocovariance function $G(\tau)/\langle I \rangle$ for out-of-phase scattering at two different temperatures. The statistical noise term at $\tau=0$ has been removed, since it contains no information about the kinetics.³ The temperature dependence of $G(\tau)$ is obvious in Fig. 4. As the temperature increases the size of the signal increases, while the decay of $G(\tau)$ becomes faster. This is the expected

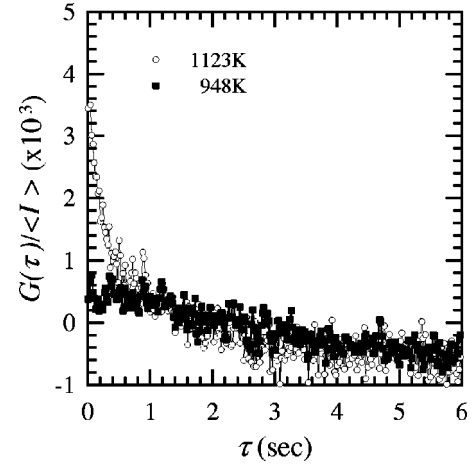


FIG. 4. Normalized autocorrelation function $G(\tau)/\langle I \rangle$ vs time for an out-of-phase condition. (○) $T = 1123 \text{ K}$. (■) $T = 948 \text{ K}$.

result caused by the larger fluctuations of the steps and the faster kinetics at higher temperatures.

To determine the rate-limiting kinetics, fits must be made to the experimental correlation functions using Eq. (5). To do this we must take into account the effects of a finite collection time. Note that the autocovariance function in Fig. 4 decays to a constant less than zero. This behavior is due to the finite collection time in the experiment. That is, the measured autocovariance function $\hat{G}(\tau)$ is only an estimate of the infinite collection time autocovariance function $G(\tau)$.¹⁰ It can be shown that for $t_c > 15\tau_{1/2}$ the measured autocovariance function for lag times less than $\sim 0.5t_c$ is simply the true correlation function minus a constant. The constant is *not* arbitrary, but depends on $G(\tau)$ and the collection time.¹⁰ For details on how to calculate this constant, the reader is referred to Ref. 10. As it turns out, the value of the calculated background varies by less than a factor of 2 when n in Eq. (5) changes from 1 to 4. To test the sensitivity of fits to Eq. (5), we allowed the background to vary by as much as a factor of 4 from the calculated value. We find that the quality of the fits (i.e., the fitted value of n) was not affected by this range of background around the calculated background determined by $t_{1/2}$ and the assumed form for $G(\tau)$.

The best-fit value for the exponent n for all the data was $n = 3.9 \pm 0.5$. This is close to $n = 4$, suggesting SD kinetics. An example of these fits is shown in Fig. 5(b), with the background-corrected correlation function shown in Fig. 5(a). The data are plotted as $\log G(\tau)$ versus $\tau^{1/4}$ to emphasize the poor fit to an exponential ($n = 1$). The fact that the data cannot be fit to $n = 1$ excludes the EC process as the rate-limiting kinetics (at least for $950 \text{ K} < T < 1130 \text{ K}$). On the other hand, the χ^2 values for an $n = 4$ fit were only slightly better than those for $n = 3$. This means that while the SD model is a better representation of the data, we cannot rule out the TD model on the bases of the fits alone. However, as we will show below, energetic arguments further support step-edge diffusion as the rate-limiting kinetics.

To determine activation energies and prefactors for the microscopic process, note that the decay times $\tau_{1/2}$ of $G(\tau)$ represent a macroscopic equilibration time of the step shape.

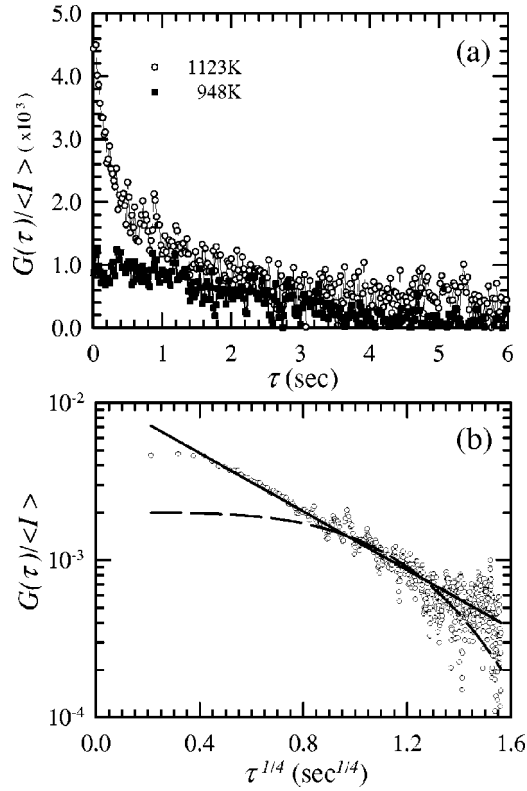


FIG. 5. Normalized autocorrelation function $G(\tau)/\langle I \rangle$ plus the best-fit background vs time for an out-of-phase condition. (○) $T = 1123$ K. (■) $T = 948$ K. (b) $\log G(\tau)/\langle I \rangle$ vs $\tau^{1/4}$ for $T = 1123$ K. (○) data. The solid and dashed lines are the best fit for the SD and EC models, respectively.

To find the microscopic time τ_x for a local fluctuation of the step, a scaling relation between $\tau_{1/2}$ and τ_x must be known. These relations have been developed from numerical calculations for different kinetic models.¹¹ However, reasonable analytical relations can be developed as long as the LEED instrument resolution ζ is much larger than the correlation length along a step edge ξ , which is the case in these experiments.^{11,24}

For SD kinetics an approximate relationship can be taken from Bartelt *et al.* for the short time growth of the mean squared step fluctuation,¹²

$$w^2(t) \approx w_\infty^2 \left(\frac{(0.464)^4 (kT)^3 \Omega^{5/2} t}{\tilde{\beta}^3 w_\infty^8 \tau_s} \right)^{1/4}, \quad (7)$$

where $\tau_s = \Omega/D_s$ is approximately the time for an atom to hop between adjacent step sites.

Making the assumption that the argument in Eq. (7) is approximately 1 when $t \rightarrow \tau_{1/2}$, and using Eqs. (4a) and (4b) gives the scaling relation

$$\tau_{1/2} \approx 1.35 \left(\frac{\xi}{a_{\parallel}} \right)^2 \left(\frac{kT}{2c} \frac{1}{\Omega^{1/2} D_s} \right). \quad (8)$$

Equation (8) is in good agreement with the numerical results of Ref. 11 in the limit $\zeta/\xi > 1$.

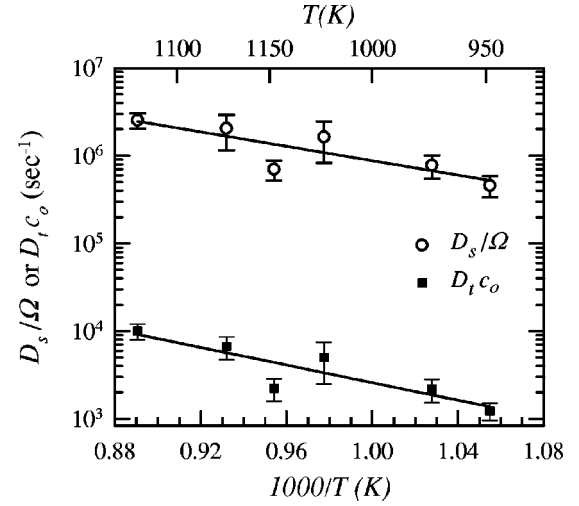


FIG. 6. An Arrhenius plot of the diffusion constants for step-edge diffusion D_s/Ω (○) and terrace diffusion $D_t c_o$, (■).

For the TD model we again use the results of Bartelt *et al.*,¹³ to cast $w^2(t)$ in a form similar to Eq. (7):

$$w^2(t) \approx w_\infty^2 \left(\frac{2^7 (kT)^2 \Omega^2}{3^{3/2} \Gamma^3(\frac{1}{3}) \tilde{\beta}^2 w_\infty^6} D_t c_o t \right)^{1/3}. \quad (9)$$

Again, defining $\tau_{1/2}$ as the time when the argument in Eq. (9) is ~ 1 , we find

$$\tau_{1/2} \approx 0.054 \left(\frac{\xi}{a_{\parallel}} \right) \left(\frac{kT}{2c\Omega^{3/2}} \frac{1}{D_t c_o} \right). \quad (10)$$

Using the experimental values of $\tau_{1/2}$ from $G(\tau)$ and experimental values of c and ξ obtained from the profile fits, we can calculate the microscopic kinetics parameters. Even though the functional time decay of the measured correlation function suggest SD kinetics, for argument sake we have calculated both D_s or $(D_t c_o)$ assuming SD or TD kinetics, respectively, from Eqs. (8) or (10). The Arrhenius plots of D_s/Ω and $D_t c_o$ are shown in Fig. 6. Assuming D_s for SD kinetics is given by $D_s = D_{s,o} \exp(-\Delta E_s/kT)$, where $\nu_s = D_{s,o}/\Omega$ and ΔE_s is the activation energy, we find $\Delta E_s = 0.8 \pm 0.2$ eV and $\nu_s \sim 1 \times 10^{10 \pm 2} \text{ s}^{-1}$.

For the case of TD kinetics, we can similarly write $1/D_t c_o = (1/\nu_t) \exp(\Delta E_t/kT)$, where ΔE_t is the sum of a diffusion barrier and a formation energy, and ν_t is the attempt frequency for diffusion. For TD kinetics we find $\Delta E_t = 1.0 \pm 0.2$ eV and $\nu_t \sim 3 \times 10^{8 \pm 2} \text{ s}^{-1}$. Note that ΔE is model dependent through the temperature dependence of ξ in Eqs. (8) and (10).

The low ΔE 's we measure support the claim that SD and not TD kinetics are the rate-limiting processes. This is because the TD activation energy should be due to both diffusion and a formation barriers: $\Delta E_t = \Delta E_D + \Delta E_F$. For Si(001) the diffusion barrier is known to be ~ 0.67 eV for monomers²⁵ and ~ 0.94 eV for dimers.²⁶ This implies that

our measured value is $\Delta E_F \sim 0.1\text{--}0.3\text{ eV}$, well below the theoretical dimer formation energy of 1.6 eV .²⁷

The same conclusion is supported from Ostwald ripening experiments on Si(001), where the time evolution of elliptically shaped islands were monitored at 970 K .²⁸ Those experiments find that the islands preserve their shape, and that no boundary fluctuations are seen within the video acquisition rate ($\Delta t \sim 1\text{ sec/frame}$). This implies that step-edge diffusion is sufficiently fast around the island perimeter to equilibrate any deviations from the smooth elliptical shape. We can estimate a lower bound on D_s by assuming diffusion around the perimeter of an elliptical island of area A is of the order of the video acquisition speed, i.e., $D_s > 4\pi A/2\Delta t$. Using $A = 2.5 \times 10^4\text{ nm}^2$ from Fig. 3 in Ref. 28, we estimate $D_s = 3 \times 10^5\text{ nm}^2/\text{sec}$ from the ripening experiments. An extrapolation of our Arrhenius parameters from Fig. 6 to 970 K gives $D_s = 2.4 \times 10^5\text{ nm}^2/\text{sec}$, in excellent agreement with the ripening results. This agreement further supports the assertion that step-edge diffusion is indeed the rate limiting microscopic mechanism deduced from our TLS experiment.

IV. DISCUSSION

The main result of this study is that the equilibrium fluctuations of S_B steps on Si(001) are not limited by the attachment or detachment of atoms or dimers from the step edge in the temperature range $950\text{ K} \leq T \leq 1130\text{ K}$. Instead, diffusion of atoms along the steps is the rate-limiting process. This result is different from those determined from both LEEM studies of Si(001) step dynamics⁸ and Ostwald ripening studies of islands on Si(001).²⁸ In both these experiments attachment/detachment of atoms or dimers from the steps was found to be the rate-limiting process. Although it seems that the conclusions drawn from our study contradict those from earlier work, a reexamination of how the time scale for different microscopic processes can overlap in different temperature ranges can reconcile these differences. In fact, as we now discuss, these differences can be reconciled in a way that gives a clearer picture of the dynamics of steps on this surface.

Equilibrium LEEM measurements on stepped Si(001) with average terrace widths of 1300 \AA have been analyzed using the same continuum model for step motion we have used to analyze our data.⁸ In that work the time-resolved Fourier components of the step shape are measured. From these measurements the time constants $\tau(q)$ and amplitude $A(q)$ for each component can be measured. In the continuum model these are given by

$$A(q) = \frac{2kT}{L\tilde{\beta}q^2}, \quad (11a)$$

$$\frac{1}{\tau(q)} = \frac{\Gamma\tilde{\beta}q^2}{2kT} \left(\frac{2c_oD_t\Omega^2q + \Omega^{3/2}D_sq^2}{\Gamma + 2c_oD_t\Omega^2q + \Omega^{3/2}D_sq^2} \right). \quad (11b)$$

The q^{-2} dependence of the amplitude has been confirmed by LEEM, supporting the validity of the continuum model.⁸ This is again consistent with STM results measuring terrace width distribution.²⁰

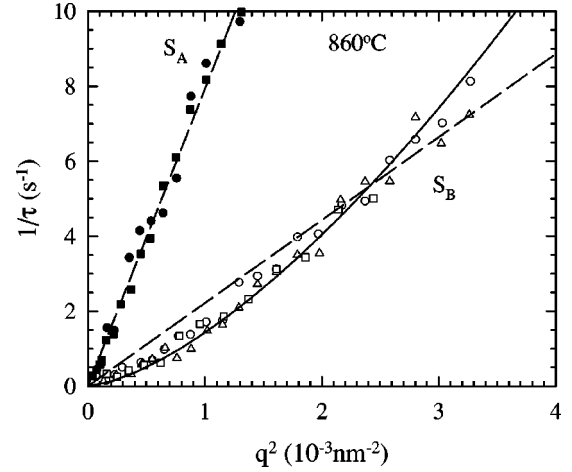


FIG. 7. $1/\tau(q)$ for both S_A and S_B steps from Si(001) taken from Ref. 8. The dashed lines are q^2 fits to the data. The solid line is a q^3 fit to the S_B step time constants.

In LEEM the rate-limiting kinetics is identified by noting the q dependence of $\tau(q)$, which from Eq. (11b) is determined by the relative magnitude of the three terms Γ , $2c_oD_t\Omega^2q^2$, and $\Omega^{3/2}D_sq^2$. For example, if attachment/detachment (EC kinetics) from steps is the rate-limiting process, i.e., Γ is much less than either $2c_oD_t\Omega^2q^2$ or $\Omega^{3/2}D_sq^2$, then $1/\tau(q) \propto q^2$. In Fig. 7 we reproduce Fig. 6 from Ref. 8, showing the q dependence of $1/\tau(q)$. For the S_B step it is not clear that $1/\tau \propto q^2$ is the only possible fit to the LEEM data. To illustrate this, we plot $1/\tau \propto q^3$ for the S_B step (solid line) in Fig. 7. It is clear that a q^3 dependence, if not a better fit, is as least as good as a q^2 dependence for the S_B step. This is particularly important because, as mentioned in Sec. III A, the TLS experiment is more sensitive to the fluctuations of the “rough” S_B step. We also point out that the range of q 's in Fig. 7 extend to larger values for S_B data than for S_A data, making the accuracy for the proposed fit better.

The q^3 fit to the LEEM data in Fig. 7 suggests that terrace diffusion is comparable to or slower than attachment kinetics. This is also evident in Fig. 9 of Ref. 8, where Bartelt and Tromp plotted $LA(q)/\tau(q)$. From Eqs. (11a) and (11b) this ratio should be a constant in q for EC kinetics or linear in q for terrace diffusion limited kinetics. While error bars are large in those measurements, it seems clear that between $790^\circ\text{C} < T < 1028^\circ\text{C}$ Fig. 9 of Ref. 8 shows evidence of a q -dependent ratio $LA(q)/\tau(q)$. These observations lead us to the conclusion that in the temperature range $790^\circ\text{C} < T < 1028^\circ\text{C}$ EC kinetics are at best comparable to terrace diffusion kinetics.

If TD and EC kinetics are comparable, as we interpret from the LEEM results, why do we measure SD kinetics in a temperature regime that overlaps with the LEEM experiments? We believe the answer is that the rate-limiting kinetics crosses over from terrace diffusion to step-edge diffusion below approximately 1070 K . In fact there is already evidence for this in the LEEM data. The Arrhenius plot of Bartelt and Tromp (Fig. 10 of Ref. 8) becomes nonlinear for $T \sim 1070\text{ K}$. Below this temperature the slope of their plot gives an activation energy of $\sim 0.9\text{ eV}$. This number is within

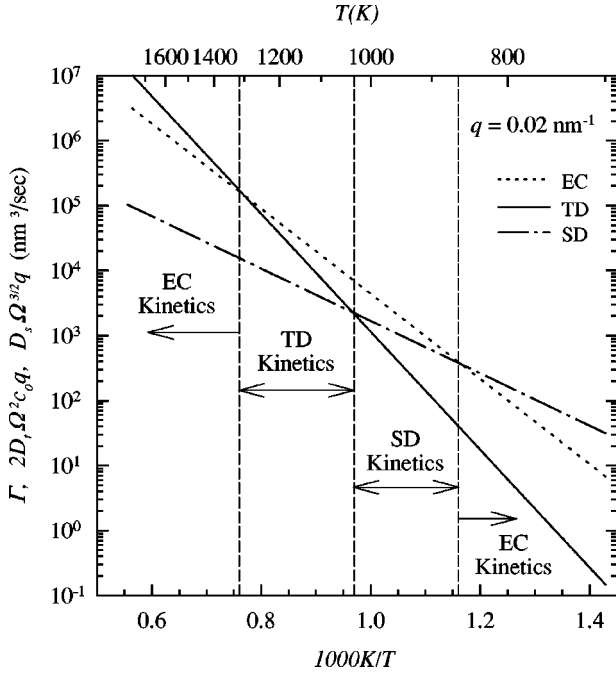


FIG. 8. Estimated rates for EC, TD, and SD kinetics vs $1/T$ as described in text. The q vector was chosen to be 0.02 nm^{-1} . Vertical dashed lines mark crossovers from one type of kinetics to another.

error bars of our value for step diffusion ($\Delta E_s = 0.8 \pm 0.2 \text{ eV}$) measured for temperatures below 1070 K .

To see that the suggestion of a crossover is plausible, we have plotted estimates of Γ , $2c_oD_t\Omega^2q$, and $\Omega^{3/2}D_sq^2$ for the three types of kinetics on an Arrhenius plot in Fig. 8 using activation energies and prefactors from both the literature and from our TLS measurements. Since these terms are q dependent, we have chosen a value $q = 0.02 \text{ \AA}^{-1}$ that is close to the instrumental resolution along the step. For EC kinetics we use STM results from step-edge detachment rates that give $\Delta E \sim 1.3 \text{ eV}$.²⁹ We pick a prefactor for detachment of 10^{11} sec^{-1} that is midrange of those reported.²⁹ For step diffusion we use our activation energies and a prefactor of 10^{12} . Finally, we can estimate the terrace diffusion coefficient by reinterpreting the LEEM results from Ref. 8 as having a significant terrace diffusion term, as suggested in Fig. 7. Using the EC and SD barriers and prefactors mentioned above, we estimate $\Delta E_T \sim 1.8 \text{ eV}$ with a prefactor of 10^{15} sec^{-1} from Fig. 9 of Ref. 8. This estimate for the TD kinetics parameters is consistent with numbers determined by LEED for relaxation of strained steps on Si(001) ($\Delta E_T \sim 2.2 \pm 0.3 \text{ eV}$ and a prefactor of 10^{14}).²²

Because of the differences in activation energies for the three processes, there are crossovers to different rate-limiting kinetics for different temperature intervals, as shown in Fig. 8. Above $\sim 1500 \text{ K}$, Fig. 8 predicts that the kinetics are detachment limited. Between 1500 and 1000 K the kinetics become more and more limited by terrace diffusion. Between 1000 and 800 K , step diffusion limits the kinetics. Below 800 K , detachment kinetics again becomes rate limiting. This scenario is consistent with both our findings, the Ostwald ripening studies and the reinterpreted LEEM results. Of course this sequence of crossovers is strongly dependent on

the exact prefactors and activation energies used to generate Fig. 8. Furthermore, the number and values of the crossover temperatures depend on the values of q used for the calculations. The point of this discussion is to show that the kinetics of steps can be very complicated, and requires exact details of both prefactors and activation energies over a very broad temperature range. What can be said for certain is that, in the region between $950 \text{ K} \leq T \leq 1130 \text{ K}$, detachment kinetics is not the rate-limiting process.

It is worth noting that Fig. 8 shows an example of the relative rates of *equilibrium* step kinetics. Inferring the kinetics for ripening experiments from Fig. 8 requires caution. In general, growth kinetics of islands far from equilibrium can be very different from near-equilibrium step kinetics. For instance, diffusion on the terraces is highly anisotropic; diffusion perpendicular to the dimer rows is at least 10^3 times slower than along the rows.⁶ Ripening requires mass transport from one island to another, while step fluctuations require mass transport along the step. For S_B steps mass transport for island growth is along the dimer rows, while for S_B step fluctuations, mass must be transported along the slow direction perpendicular to the dimer rows. Therefore, while detachment kinetics may limit island growth, S_B step fluctuations may be limited by the slower terrace diffusion process required to transport mass along the step (at least in some temperature region).

Furthermore the crossover regimes between different kinetics depend on the relevant wave vector q that is set by the experimental probe or, as in the ripening experiment, by the island size. The ripening experiments are sensitive to large wave vectors defined by $q > q_c \sim 1/R$, the inverse of the island size (especially at early times). In addition, because the perimeter of the growing island consists of a mixture of both types of steps, the total kinetics is sensitive to the dynamics of both S_A and S_B . Both features favor atom detachment for island ripening. On the other hand, the TLS experiment reported here monitors fluctuations on long steps (limited only by the instrumental resolution along the steps) and, as discussed in Sec. III A, is more sensitive to fluctuations of the S_B step. Both conditions favor a mechanism different from atom detachment, and as argued earlier, indicate that step diffusion is the controlling rate.

Finally, pure detachment kinetics in the island ripening experiments may be a simplification of the system dynamics. The time dependence of the island size is related to the q dependence of $\tau(q)$. For EC kinetics, $\tau(q) \propto q^{-2}$ gives rise to a linear time dependence as seen in the ripening experiments. In addition to its q dependence, $\tau(q)$ also scales with the mean step separation L through the correlation length ξ and the step-step interaction c .³⁰ For SD kinetics, Eq. (10) predicts that $\tau_{1/2}$ scales as ξ^2/c , which, from Eq. (4b), is proportional to $1/c^2$. Since c scales as L^{-2} , $\tau_{1/2} \propto L^4$. Similarly for TD kinetics, $\tau_{1/2} \propto L^3$. For EC kinetics, $\tau_{1/2} \propto 1/c \propto L^2$.¹² If the island growth rate was limited by EC kinetics, we would expect an L^2 dependence on the time constant. However, Webb *et al.*²² found a linear L scaling of step equilibration time for $T \sim 790 \text{ K}$, inconsistent with all three models presented so far.

In fact the result of Webb *et al.*²² is more consistent with another model for step kinetics proposed by Pimpinelli, Heyraud, and Mètois.³⁰ They proposed a modification to the terrace diffusion kinetics discussed in Sec. I. Rather than diffusion across the terrace from one point on the step to another, the source of atoms or dimers comes from neighboring steps that subsequently diffuse to the step edge. In this form of terrace diffusion $\tau(q) \propto Lq^2$, predicting a linear L dependence on the step equilibration time as observed by Webb *et al.*²²

V. CONCLUSION

We have shown how temporal LEED spectroscopy can be used to measure the dynamics of surfaces. As a specific example, we have studied the kinetics of stepped Si(001). We have shown that the rate-limiting kinetics can be identified, and that both kinetic barriers and prefactors can be measured. The main result of this work is that the diffusion of atoms or dimers along the S_B step edge is the rate-limiting process that determines the equilibrium fluctuation of the S_B steps on Si(001) in the temperature region $950 \text{ K} \leq T \leq 1130 \text{ K}$. We find that the activation energy for step-edge diffusion is $\Delta E_s = 0.8 \pm 0.2 \text{ eV}$, with a hopping rate of $\nu_s \sim 1 \times 10^{10 \pm 2} \text{ s}^{-1}$.

Comparing our findings with the work of others who also studied the dynamics of this surface, at both lower and

higher temperatures, indicates that the dynamics of steps on Si(001) is quite complicated. Differences between LEEM findings and the TLS results reported here can be reconciled if all experimental factors controlling the experiment (i.e., temperature, wave vector, type of step) are taken into account. This is especially true since a single dynamic mechanism only operates over a finite-temperature range. One important conclusion from our study is that it is essential to cover a wide range of controlling variables to be able to identify the crossover regions. This is the only way to make comparisons between different experiments meaningful. It is not only an oversimplification to state the type of microscopic mechanism operating in an experimental system, in this case Si(100), but confusing as well, since the dominant system dynamics depends drastically on many factors that change from one experiment to another. Instead, it is more accurate to compare the Arrhenius parameters extracted in different experiments (i.e., activation energy and prefactors) for the different microscopic mechanisms irrespective of the temperature range of the experiment.

ACKNOWLEDGMENTS

Ames Laboratory is operated for the U.S. Department of Energy by Iowa State University under Contract No. W-7405-Eng-82 (M. T.). This work was supported in part by the NSF under Grant No. DMR-9211249 (E. C.).

-
- ¹I. S. Hwang, S. K. Theiss, and J. Golovchenko, *Science* **265**, 490 (1994).
- ²R. Gomer, in *Surface Diffusion Atomic and Collective Processes*, Vol. 360 of *NATO Advanced Study Institute, Series B*, edited by M. C. Tringides (Plenum, New York, 1997) pp. 427–442.
- ³E. H. Conrad, A. Menzel, S. Kiriukhin, and M. C. Tringides, *Phys. Rev. Lett.* **81**, 3175 (1998).
- ⁴B. S. Swartzentruber, Y.-W. Mo, R. Kariotis, M. G. Lagally, and M. B. Webb, *Phys. Rev. B* **65**, 1913 (1990).
- ⁵H. J. Zandvliet, H. B. Elswijk, and E. J. van Loenen, *Surf. Sci.* **272**, 264 (1992).
- ⁶D. Dijkkamp, E. J. van Loenen, and H. B. Elswijk, in *Ordering at Surfaces and Interfaces*, edited by A. Yoshimori, T. Shinjo, and H. Watanabe (Springer-Verlag, Berlin, 1992), p. 85.
- ⁷C. Pearson, B. Borovsky, M. Krueger, R. Curtis, and E. Ganz, *Phys. Rev. Lett.* **74**, 2710 (1995).
- ⁸N. C. Bartelt and R. M. Tromp, *Phys. Rev. B* **54**, 11 731 (1996).
- ⁹E. H. Conrad, in *Physical Structures*, edited by W. N. Unertl Handbook of Surface Physics Vol. 1 (Elsevier, Amsterdam, 1996), pp. 271–360.
- ¹⁰A. Menzel, E. H. Conrad, and M. C. Tringides (unpublished).
- ¹¹A. Menzel, K. Wiesenfeld, E. H. Conrad, and M. C. Tringides, *Phys. Rev. B* **61**, 2997 (2000).
- ¹²N. C. Bartelt, J. L. Goldberg, T. L. Einstein, and E. D. Williams, *Surf. Sci.* **273**, 252 (1992).
- ¹³N. C. Bartelt, T. L. Einstein, and E. D. Williams, *Surf. Sci.* **312**, 411 (1994).
- ¹⁴N. C. Bartelt, T. L. Einstein, and E. D. Williams, *Surf. Sci.* **276**, 308 (1992).
- ¹⁵N. C. Bartelt, T. L. Einstein, and E. D. Williams, *Surf. Sci. Lett.* **240**, L591 (1991).
- ¹⁶P. Nozières, in *Solids Far From Equilibrium*, edited by C. Godrèche (Cambridge University Press, Cambridge, 1991), p. 1.
- ¹⁷The $n=3$ form of $G(\tau)$ has not been derived explicitly for the TD model. It can be justified by analogy since the time constant, $\tau(q)$, for a Fourier component of the fluctuation is proportional to q^{-4} and q^{-3} in the SD and TD models, respectively (Ref. 8).
- ¹⁸K. D. Gronwald and M. Henzler, *Surf. Sci.* **117**, 180 (1982).
- ¹⁹B. S. Swartzentruber, Y.-W. Mo, M. B. Webb, and M. G. Lagally, *J. Vac. Sci. Technol. A* **7**, 2901 (1989).
- ²⁰B. S. Swartzentruber, N. Kitamura, M. G. Lagally, and M. B. Webb, *Phys. Rev. B* **47**, 13 432 (1993).
- ²¹N. C. Bartelt, R. M. Tromp, and E. D. Williams, *Phys. Rev. Lett.* **73**, 1656 (1994).
- ²²M. B. Webb, K. K. Men, B. S. Swartzentruber, R. Kariotis, and M. G. Lagally, *Surf. Sci.* **242**, 23 (1991).
- ²³O. L. Alerhand, David Vanderbilt, Robert D. Meade, and J. D. Joannopoulos, *Phys. Rev. Lett.* **61**, 1973 (1998).
- ²⁴M. Kammler *et al.*, in *Collective Surface Diffusion Coefficients under Non-Equilibrium Conditions*, Vol. 29 of *NATO Advanced Study Institute, Series II*, edited by M. C. Tringides and Z. Chvoj (Kluwer, Dordrecht, 2001).
- ²⁵Y.-W. Mo, J. Kleiner, M. B. Webb, and M. G. Lagally, *Phys. Rev. Lett.* **66**, 1998 (1991); *Surf. Sci.* **268**, 275 (1992).
- ²⁶B. S. Swartzentruber, *Phys. Rev. Lett.* **76**, 459 (1996).
- ²⁷A. Rockett, *Surf. Sci.* **312**, 201 (1994).
- ²⁸N. C. Bartelt, W. Theis, and R. M. Tromp, *Phys. Rev. B* **54**, 11 741 (1996).
- ²⁹B. S. Swartzentruber, and M. Schacht, *Surf. Sci.* **322**, 83 (1995).
- ³⁰A. Pimpinelli, Heyraud, and J. J. Mètois, *Surf. Sci.* **295**, 143 (1993).